Oxidation Kinetics of a Lime-Copper Concentrate Pellet

H. H. HAUNG AND R. W. BARTLETT

Copper flotation concentrates can be oxidized while simultaneously fixing 98 pct of the sulfur as $CaSO_4$ and copper sulfates if a mixed lime-concentrate balled pellet is roasted at low temperatures. The roasting pellet exhibits a reacted shell surrounding the unreacted core. The rate is controlled by oxygen diffusion in the pores of the roasted shell and kinetic details are given. At higher temperatures the rate decreases because of sintering and decreased porosity in the shell. Complete roasting of the pellets while controlling the pellet temperature to prevent formation of insoluble copper ferrites is required for subsequent hydrometallurgical extraction.

PROCESSES for treating sulfide-copper flotation concentrates that do not cause appreciable air pollution by SO_2 emission are needed. The recently developed lime-concentrate-pellet-roast (LCPR) process[1] involves roasting a mixture of finely ground flotation concentrates and nearly stoichiometric lime in the form of a balled pellet followed by leaching in sulfuric acid and eventual recovery of copper by electrowinning. Pelletization is necessary to retain nearly all of the sulfur as anhydrite ($CaSO_4$) during roasting.

When a pellet is roasted, oxidation of the sulfide mineral grains occurs at the interface separating the unreacted pellet core from a roasted shell, provided that the mineral particles are not too large. Although −200 mesh concentrates were used in these experiments, concentrates as coarse as 35 mesh have been successfully treated. The reaction products are primarily CuO, Fe_2O_3 and $CaSO_4$. If a substoichiometric amount of lime is used at low temperatures, some $CuSO_4$ and $CuO \cdot CuSO_4$ will also be produced. At high roasting temperatures some copper ferrite is formed. Sulfur dioxide gas is produced by the roasting reaction and diffuses out of the pellet through pores in the reaction product shell. The diffusing SO_2 reacts with lime in a diffuse zone adjacent to the core/shell interface. Although less than 5 pct of the SO_2 escapes the pellet under normal roasting conditions, the SO_2 that does escape originates predominantly from near the surface of the pellet early in the roasting period, when the roasted shell through which diffusion must occur is very thin.

The purpose of the present study is to report on the single pellet roasting kinetics.

The roasting reactions and the lime reaction with SO_2 are exothermic and may cause overheating and formation of copper ferrite which is relatively insoluble in a sulfuric acid leach.[2] For industrial scaleup, consideration should be given to a continuously fed fluid bed roaster with water injection to obtain temperature control and temperature uniformity throughout the bed.

H. H. HAUNG, formerly Graduate Student, Stanford University, has a Post Doctoral Research Appointment, University of Utah, Salt Lake City, UT. R. W. BARTLETT, formerly Associate Professor, Stanford University, is now with Kennecott Copper Corporation, Salt Lake City, UT.

Manuscript submitted March 11, 1974.

EXPERIMENTAL METHODS

Experiments reported here were limited to flotation concentrates originating at Bingham, Utah in which chalcopyrite was the primary copper mineral. The assay was 24.2 pct copper, 21.1 pct iron and 26.0 pct sulfur. Reagent lime was thoroughly mixed with −200 mesh concentrate with the amount of lime varied from 85 pct to 100 pct of the amount required to convert all of the sulfur in the charge to $CaSO_4$. Water was added and pellets were balled in a 28 cm diam laboratory balling drum.

The optimal moisture content for pelletizing was 14 pct. Average drum residence time for 1.1 cm pellets was 20 to 30 min, and the undersize pellets were recharged as seeding to the drum.

Single pellet kinetics were determined using a quartz spring balance thermogravimetric analyzer shown in Fig. 1, which measured both the weight gain associated with roasting and the SO_2 lime fixation reaction. Sulfur dioxide in the effluent gas was continuously measured by an infrared analyzer during the entire TGA oxidation experiment. A single pellet, suspended from a quartz helix spring having a sensitivity of ±0.16 mg, was heated to the desired temperature in a 6.5 cm ID tube furnace while the dehydration of lime occurred in an inert atmosphere. After dehydration was complete, the desired oxygen composition was introduced and the weight gain due to the oxidation and sulfation of the pellet was followed as a function of time. For each run the quartz balance was continuously observed after inserting oxygen until the initial weight change was observed at which time the timer was started, $t = 0$. An initial weight change of 0.05 pct of the final weight change was detectable. For each run, the infrared results were calibrated by absorbing all of the SO_2 in sodium hydroxide solution and titrating with the iodine method.

Up-draft fixed bed roasting experiments were conducted to observe thermal effects and determined maximum bed depths that could be used without overheating. An air or air/nitrogen mixture was preheated in a vertical tube furnace and flowed through a grate into an insulated stainless steel cup holding the pellets. Bed depths up to 18 cm were used and thermocouples were inserted at various depths in the bed. Thermocouples were also buried in pellets within the bed. The gas flow velocity was regulated at room temperature through flow meters, before entering the preheat

furnace. Since effluent gases contained negligible SO_2 they were vented into the laboratory.

Apparent densities of pellets were determined before and after roasting by immersion in mercury. Porosities of roasted pellets were determined by benzene absorption. Measured values of volume shrinkage on roasting and final fired porosities at various temperatures are shown in Fig. 2. All of the shrinkage at higher temperatures occurred on heating prior to insertion of the oxidizing atmosphere. Although the data shown in Fig. 2 are appropriate to this particular study and reasonably typical, it should be noted that pellet porosity will also depend on the amount of lime, the particle size distributions of lime and concentrate, the ball forming conditions and densification. The specific surface of roated pellets was determined by the BET nitrogen adsorption method.

Pellet strength is very important for industrial processing. A suitable green pellet should withstand[3] an average of 6 drops from 45 cm onto a steel plate and have a minimum crushing strength of 1.5 kg. The laboratory balled pellets surpass these requirements.

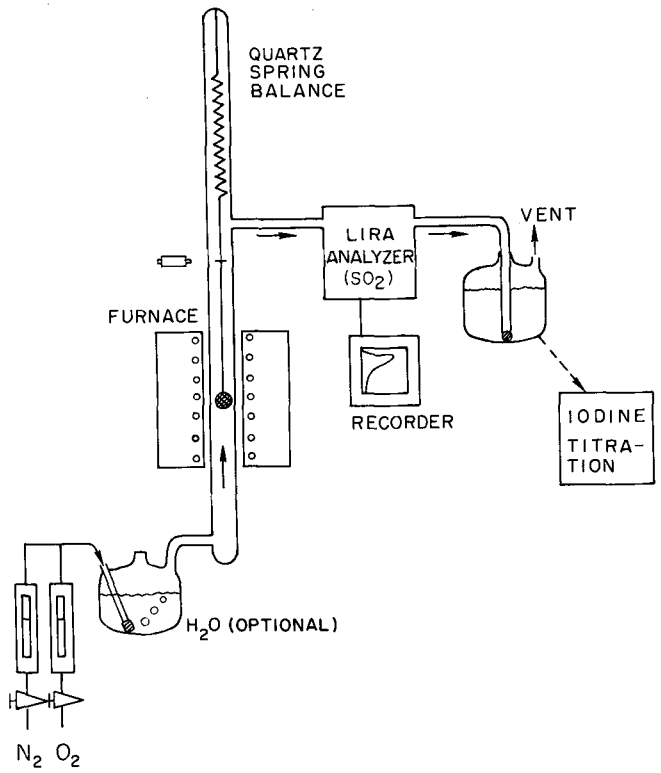

Fig. 1—Combined thermogravimetric and infrared apparatus for analysis of single pellet oxidation kinetics.

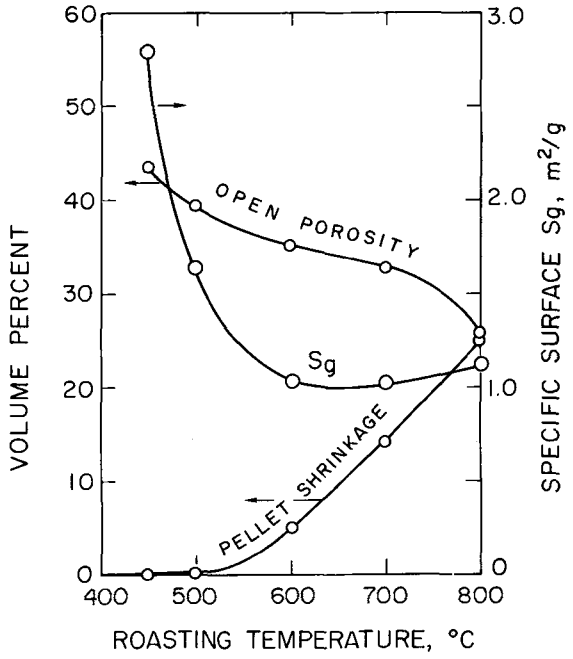

Fig. 2—Physical characteristics of roasted LCPR pellets.

SINGLE PELLET EXPERIMENTAL RESULTS AND REACTION MODEL VERIFICATION

Typical weight gain curves for 1.15 cm diam balled pellets are shown in Fig. 3 for air roasting at 450°C and in Fig. 4 for air roasting at 800°C. The measured weight gain is shown with the weight associated with the SO_2 gaseous effluent determined from infrared measurements. The total weight gain for solid and gaseous products is also shown and these will be referred to as total rate curves. The emission of SO_2 increases with temperature.

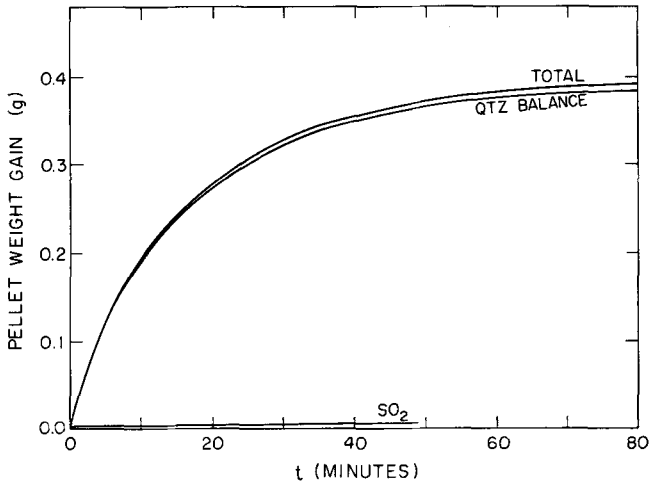

Fig. 3—Single pellet oxidation weight change at 450°C.

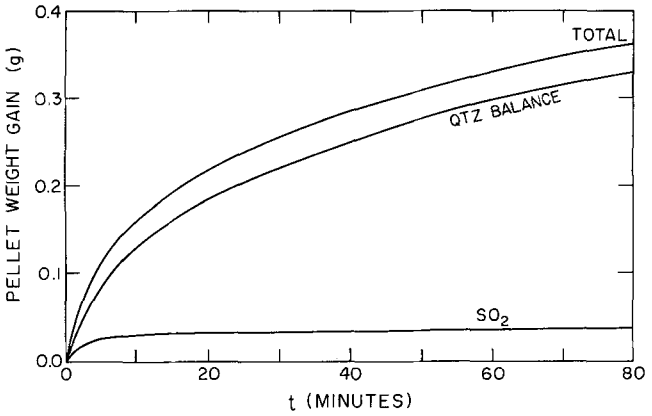

Fig. 4—Single pellet oxidation weight change at 800°C.

The experimental kinetic curves were analyzed in terms of an oxygen transport rate limiting model. Initially, oxygen transfer through the boundary layer gas film surrounding the pellet is rate controlling. A convective oxygen diffusion gradient in residual nitrogen occurs. Over most of the reaction period oxygen diffusion through pores in the roasted shell is rate controlling. This reaction model is illustrated in Fig. 5.

Boundary Layer Gas Film Oxygen Transfer

Initial tangents ($t \rightarrow 0$) to the total rate curves were measured and used to determine the initial oxidation rate of the pellet, $\dot{W}_p$. From these data, experimental values of the initial mass transfer coefficients were determined from the relation,

$$\dot{W}_p \Big|_{t=0} = k_m 4\pi r_p^2 (C_{O_2}{}^{(g)} - C_{O_2}{}^{(o)}) \simeq k_m 4\pi r_p^2 C_{O_2}{}^{(g)} \quad [1]$$

and

$$\frac{\Delta W_p}{4\pi r_p^2} = k_m C_{O_2}{}^{(g)} t . \quad [2]$$

Initial mass transfer coefficients were independently calculated by two empirical correlations for mass transfer to spheres:

Froessling[4]

$$\frac{2r_p k_m}{D_{AB}} = 2.0 + 0.60\left(\frac{2r_p \rho_g U}{\mu}\right)^{1/2}\left(\frac{\mu}{\rho_g D_{AB}}\right)^{1/3} . \quad [3]$$

Steinberger and Treybal[5]

$$\frac{2r_p k_m}{D_{AB}} = 2.0 + 0.343\left(\frac{2r_p \rho_g U}{\mu}\right)^{0.62}\left(\frac{\mu}{\rho_g D_{AB}}\right)^{0.31} . \quad [4]$$

Viscosities and binary bulk diffusivities for the oxygen-nitrogen gas mixtures were calculated at the appropriate temperatures by the Chapman-Enskog formula. The air mass velocity flowing over the pellets was, $\rho_g U = 0.002$ g s^{-1} cm^{-2} in most of the experiments. The two theoretical (calculated) mass transfer coefficients and the experimental mass transfer coefficient are shown for each temperature in Table I. The experimental mass transfer coefficients at each temperature were obtained by taking the tangent at the origin ($t = 0$) and are slightly less than the calculated mass transfer coefficients. This agreement is adequate and the discrepancy may be caused by surface roughness of the pellets or the retarding effect of the pellet suspending saddle on the transfer of oxygen. The experimental apparent activation energies agree with the values for calculated rates.

Single pellet roasting rate experiments were also conducted at 500°C in the binary gas mixtures with the oxygen varying from 5 to 30 pct of the mixture with no effect on the mass transfer coefficient. The variations in the initial mass transfer coefficient were less than ± 0.03 cm s^{-1}. This result is also consistent with a boundary layer diffusion rate controlling process.

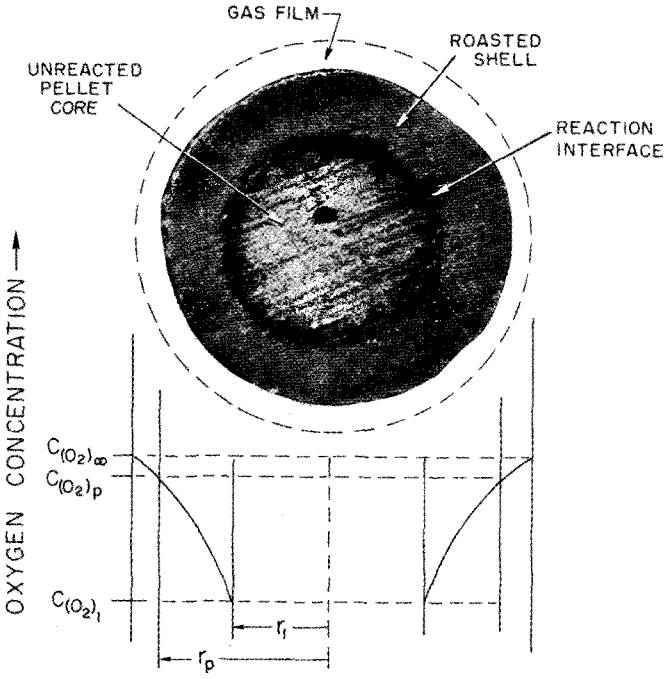

Fig. 5—Model of a roasting LCPR pellet in cross-section.

Oxygen Transfer Through the Roasted Pellet Shell

The kinetic model for most of the reaction period when shell diffusion is rate controlling is based on binary gas diffusion in a mixture of oxygen and nitrogen within a porous solid at constant total pressure. Although SO_2 is formed at the reaction interface and diffuses outward it is consumed in a diffuse zone near the interface and over most of the shell-thickness SO_2 can be neglected. The present simple model implicitly assumes that all of the chemical reaction including SO_2 fixation occurs at the core/shell interface. It is assumed that the physical characteristics of the roasted shell do not change with roasting time.

Nitrogen in the pores is stagnant and the nitrogen flux, N_B, with respect to the pellet is $N_B = 0$. The oxygen flux with respect to the pellet, N_A, takes the general form,[6]

$$N_{A_r} = \frac{-C}{\dfrac{1 - \left(1 + \dfrac{N_B}{N_A}\right) X_{A_r}}{D_{AB,\,\mathrm{eff}}} + \dfrac{1}{D_{KA,\,\mathrm{eff}}}} \frac{dX_A}{dr} \quad [5]$$

where $D_{AB,\,\mathrm{eff}}$ is the effective bulk diffusivity and $D_{KA,\,\mathrm{eff}}$ is the effective Knudsen diffusivity. Because a binary system is involved, $X_A = 1 - X_B$.

A solution to the overall reaction kinetics for a spherical pellet under conditions when transport

Table I. Experimental and Theoretical Results of Boundary Layer Oxygen Transfer Rate Controlling Step in Pellet Oxidation

k_m (cm s^{-1})	450°C	500°C	600°C	700°C	800°C	Apparent Activation Energy
Experimental	1.79	1.92	2.29	2.99	3.35	2.81 kcal mole^{-1}
Froessling[4]	2.60	2.90	3.52	4.23	5.19	3.05 kcal mole^{-1}
Steinberger and Treybal[5]	2.23	2.50	3.02	3.67	4.49	2.87 kcal mole^{-1}

through the roasted shell is rate controlling is available for the case of equimolar counter-current diffusion, $N_B = -N_A$, and the flux equation,

$$N_{A_r} = -C D_{\text{eff}} \frac{dX_A}{dr}. \quad [6]$$

For counter-current equimolar diffusion the molar flow through the shell from the surface of the core, r_l, to the outer limit of the shell, r_p, is:

$$\dot{W}_p = 4\pi r_l^2 N_{A_r}\Big|_{r=r_l} = \frac{4\pi C D_{\text{eff}} (X_{A_l} - X_{A_p})}{\frac{1}{r_l} - \frac{1}{r_p}}. \quad [7]$$

When the molar flow of oxygen $\dot{W}_p$, for bulk diffusion in stagnant nitrogen is considered, $N_B = 0$, with the condition $D_{KA,\text{eff}} \gg D_{AB,\text{eff}}$ then the solution to Eq. [5] becomes

$$\dot{W}_p \simeq \frac{4\pi C D_{AB,\text{eff}}}{\frac{1}{r_l} - \frac{1}{r_p}} \ln\left(\frac{X_{B_p}}{X_{B_l}}\right). \quad [8]$$

Hence, it can be shown that an overall effective diffusivity for use with Eq. [7] is

$$\frac{1}{D_{\text{eff}}} = \frac{1}{D_{KA,\text{eff}}} + \frac{(X_B)_{\ln}}{D_{AB,\text{eff}}} \quad [9]$$

where

$$(X_B)_{\ln} = \frac{X_{B_p} - X_{B_l}}{\ln(X_{B_p}/X_{B_l})}. \quad [10]$$

For roasting in air with $X_{B_p} = 0.79$ and oxygen depletion at the reacting interface, $X_{B_l} = 1.0$ and the logarithmic mean value of the nitrogen mole fraction is $(X_B)_{\ln} = 0.89$.

When pore volume fraction, θ, and pore tortuosity, τ, are considered for the roasted shell,

$$D_{AB,\text{eff}} = \frac{D_{AB}\theta}{\tau} \quad [11]$$

and

$$D_{KA,\text{eff}} = \frac{D_{KA}\theta}{\tau}. \quad [12]$$

Measured values of the porosity of fired pellets were used in calculating effective diffusivities while various values of the tortuosity were considered.

Bulk diffusivities for oxygen-nitrogen mixtures, D_{AB}, were calculated using,

$$D_{AB} = \frac{0.00816\sqrt{T^3\left(\frac{1}{M_A} + \frac{1}{M_B}\right)}}{p\sigma_{AB}^2 \Omega_{D,AB}} \quad [13]$$

and the appropriate Chapman-Enskog parameters.

Knudsen diffusivities for oxygen, D_{KA} were calculated[6] using the average pore radius, r_e:

$$D_{KA} = 9700\, r_e \sqrt{\frac{T}{M_A}}. \quad [14]$$

Surface area, porosity, and bulk density measurements of roasted pellets were used to determine the average pore radius,

$$r_e = \frac{2\theta}{S_g \rho_p}. \quad [15]$$

The fractional conversion of the spherical pellet during roasting, F, may be defined by noting that

$$1 - F = \frac{\text{Volume of unroasted pellet}}{\text{Total pellet volume}} = \left(\frac{r_l}{r_p}\right)^3. \quad [16]$$

Integration of the flux equation (Eq. [6]) leads to the following expression[7] in terms of fractional conversions,

$$1 + 2(1-F) - 3(1-F)^{2/3} = \frac{6 C D_{\text{eff}} (X_{A_p} - X_{A_l}) t}{(\Delta\rho_A) r_p^2} \quad [17]$$

where $\Delta\rho_A$ is the increase in molar density of oxygen resulting from complete roasting of the pellet including SO_2 fixation. The measured radius of the roasted pellet was used for r_p.

Experimental roasting data including both weight gain and SO_2 emission were used to compute $F(t)$ and $\Delta\rho_A$. These data were plotted in the form of Eq. [17], $(1 + 2(1-F) - 3(1-F)^{2/3}$ *vs* $t)$ for air roasting at several temperatures, Fig. 6. The straight line fit of these data out to nearly complete extraction support the shell diffusion model. Experimental values of D_{eff} were determined from the slopes of Fig. 6, taking $X_{A_1} = 0$.

Experimental (points) and theoretical values (curves) of the effective diffusivities for roasting in air, $X_{A_p} = 0.21$, are shown in Fig. 7. The data are presented in the form of an Arrhenius plot: log D_{eff} *vs* $1/T$. Because of decreasing porosity in the roasted pellet shell with increasing roasting temperature at the high temperature end of the temperature range investigated, a slight negative apparent activation energy is theoretically predicated and experimentally observed. Good agreement with experimental and theoretical values of the effective diffusivity were obtained but a tortuosity factor slightly greater than the usual value, $\tau = 2$, is required.

The effective diffusivity should be invariant with changes in the oxygen partial pressure and mole fraction, X_{A_p}, provided the total pressure remains constant. Experimental effective diffusivities determined at 500°C in binary gas mixtures containing from 5 pct to 30 pct oxygen are shown in Fig. 8. As expected, a

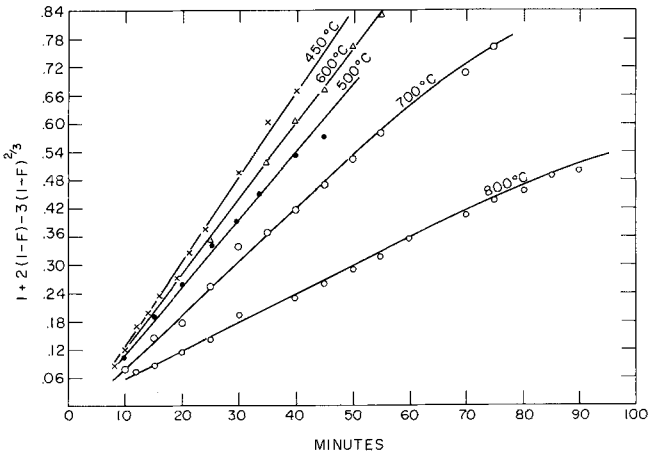

Fig. 6—Pellet roasting rate data plotted to fit a shell-diffusion model.

systematic variation in D_{eff} with oxygen concentration was not observed.

A temperature rise occurs in the pellets during roasting because of the exothermic chemical reactions. A typical temperature rise, recorded by a thermocouple imbedded at the center of the pellet is shown in Fig. 9. The gas temperature and initial pellet temperature were 500°C. A similar temperature profile has been predicted by a computer program based on the reaction rate and heat transfer considerations using a uniform pellet temperature model (instantaneous thermal conductivity in the solid). This temperature rise will increase the effective diffusivity by only 10 to 15 pct over the value calculated for the nominal roasting temperature.

DISCUSSION OF HEAT TRANSFER IN A ROASTING BED

The roasting process is extremely exothermic and heat transfer dominates the roaster design. For the overall reaction,

$$CuFeS_2 + \frac{17}{4}O_2 + 2\,CaO \rightarrow 2\,CaSO_4 + CuO + 1/2\,Fe_2O_3 \quad [18]$$

at 527°C, the heat of reaction is $\Delta H = -474{,}200$ cal per mole of $CuFeS_2$. However, heat release will vary widely between different concentrates depending on the amount of other sulfides and gangue present.

The following constraints, some based on calculations not presented here, must be summarized. The rate of heat released chemically is directly proportional to the extensive rate of chemical reaction, which because of the spherical pellet geometry and diffusion controlled reaction kinetics is greatest during the initial roasting period. The pellet temperature must be limited to prevent formation of ferrites that are relatively insoluble in leaching. The sensible heat of the pellets is only about 7 pct of the chemical heat released, or 20 pct if $Ca(OH)_2$ dehydration is included.

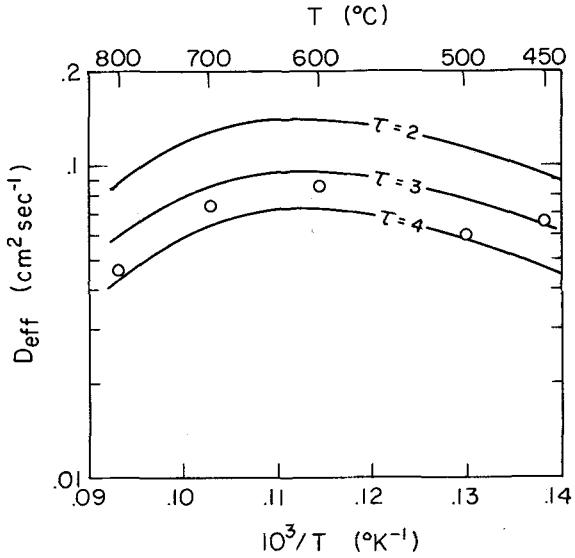

Fig. 7—Effective diffusivities for the shell-diffusion controlled roasting rate: experimentally determined points and theoretical curves.

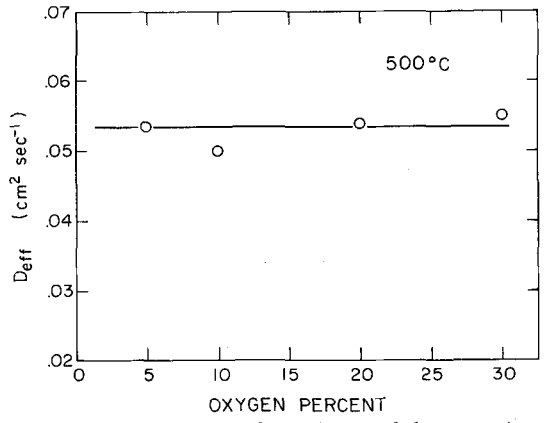

Fig. 8—Oxygen pressure independence of the experimental effective diffusivities.

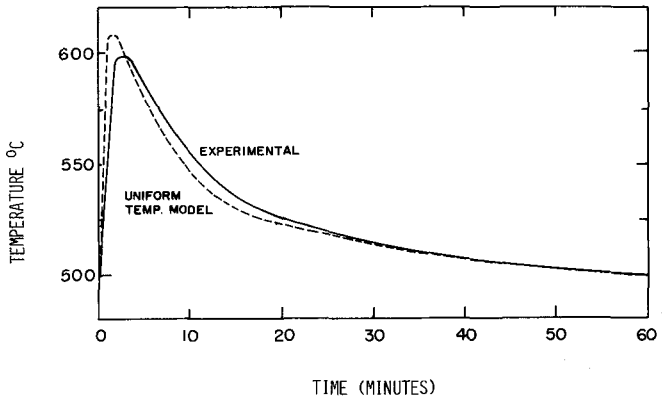

Fig. 9—Experimental and numerical results of particle temperature during the course of roasting.

Hence, the pellets are not a significant heat sink and recycle of cooled, roasted pellets will not be a practical method of eliminating the heat released.

Water injection can be used to cool a fluidized bed (well mixed solids) roaster but heat must be eliminated by transfer to the roaster gases passing through a fixed pellet bed. Large volumes of cooling gas must be used because gas heat capacities are small. For fixed bed roasters, pellet fluidization in updraft machines or a high pressure drop across the bed impose a practical upper limit on the gas velocities that can be used and this in turn limits the rate at which heat can be removed from the pellet bed and also limits the pellet bed height or thickness through which the gas is flowing. This constraint eliminates a shaft furnace process.

Increasing the pellet size radically increases the time to complete roasting, $\tau_p \propto r_p^2$, but only slightly decreases the initial (maximum) heat release rate, $\dot{Q}_{bed}\big|_{t=0} \propto r_p$, hence, increasing the pellet radius, r_p, is an unsuitable direction toward effecting adequate bed temperature control. The pellet size should be the smallest consistent with a good sulfur retention and leaching, and a practical range of sizes for industrial operating practice.

With the requirements of a short bed height and variable heat removal rates and gas velocities, a cross-current continuous process with respect to bed movement and gas flow was considered using a travel-

ing grate machine similar to that used in iron ore pelletization. High blowing rates would be required early in the roasting cycle when the maximum rate of heat release is encountered.

Alternate up-draft and down-draft gas flow cycling is not very useful. The cycle period must be very short, because of the limited sensible heat of the solids resulting from allowable temperature changes caused by alternative up-draft and down-draft flow.

Experiments, with an up-draft fixed bed pellet roaster showed that to prevent an excessive temperature excursion during the initial reaction period, the bed height must be limited to 7 to 15 cm for two concentrates studied. These results limit the practical application of a fixed bed roaster and indicate that industrial scale-up should concentrate on a continuously operated fluid bed roaster with water injection into the bed to offset the released heat and control the roasting temperature.

NOMENCLATURE

C	total gas species concentration, moles cc^{-1}
$C_{O_2}^{(o)}$	oxygen concentration at the reaction site, moles cc^{-1}
$C_{O_2}^{(g)}$	oxygen concentration in the bulk gas, moles cc^{-1}
D_{AB}	ordinary diffusion coefficient for an oxygen/nitrogen mixture, $cm^2\ s^{-1}$
$D_{AB,\text{eff}}$	effective bulk diffusion coefficient for an oxygen/nitrogen mixture in pores, $cm^2\ s^{-1}$
D_{KA}	Knudsen diffusion coefficient for oxygen, $cm^2\ s^{-1}$
$D_{KA,\text{eff}}$	effective knudsen diffusion coefficient for oxygen, $cm^2\ s^{-1}$
D_{eff}	overall effective oxygen diffusion coefficient, $cm^2\ s^{-1}$
F	volume fraction of the pellet that has been roasted
k_m	mass transfer coefficient for oxygen, $cm\ s^{-1}$
M_A	molecular weight of oxygen, M/mole
M_B	molecular weight of nitrogen, M/mole
N_A	molar flux of oxygen, moles $cm^{-2}\ s^{-1}$
N_B	molar flux of nitrogen, moles $cm^{-2}\ s^{-1}$
p	pressure, Eq. [13], atm
r	radial position in the pellet, cm
Δr	$r_p - r_l$, cm
r_e	average pore radius, cm
S_g	specific surface area of the pellet, $cm^2\ g^{-1}$
t	time, s
Δt	time increment, s
T	temperature, K
U	superficial gas velocity through the bed or around the pellet, $cm\ s^{-1}$
$\dot{W}_p$	molar rate of oxidation per pellet, moles oxygen $pellet^{-1}\ s^{-1}$
ΔW_p	finite increment of oxidation of a pellet, moles oxygen $pellet^{-1}$
X_A	mole fraction of oxygen
X_B	mole fraction of nitrogen
$(X_B)_{\ln}$	logarithmic mean mole fraction of nitrogen, see Eq. [10]
θ	pellet porosity (volume fraction)
μ	gas viscosity, $g\ cm^{-1}\ s^{-1}$
ρ_p	pellet apparent density, $g\ cm^{-3}$
ρ_g	gas density, $g\ cm^{-3}$
$\Delta\rho_A$	increase in molar density of oxygen resulting from complete roasting, moles cc^{-1}
σ_{AB}	collision diameter, Eq. [13], Å
τ	tortuosity factor for a porous solid
$\Omega_{D,AB}$	collision integral, Eq. [13].

SUBSCRIPTS

g	characteristic of the bulk gas
p	evaluated at the pellet surface, r_p
l	evaluated at the pellet reaction interface, r_l
r	evaluated at radius r.

ACKNOWLEDGMENT

Partial support of this research was contributed by the U.S. Bureau of Mines under Grant G 133085.

REFERENCES

1. R. W. Bartlett and H. H. Haung: *J. Metals*, 1973, vol. 25, no. 12, pp. 28-34.
2. F. P. Haver and M. M. Wong: *Mining Eng.*, 1972, vol. 24, no. 6, p. 52.
3. J. H. Strassberger, *et al: Blast Furnace Theory and Practice*, vol. 1, p. 286, Gordon and Breach Science Publishers, New York, 1969.
4. N. Froessling: *Gerlands Beitr. Geophys.*, 1938, vol. 52, p. 1183.
5. R. L. Steinberger and R. E. Treybal: *AIChE J.*, 1960, vol. 6, p. 227.
6. C. N. Satterfield: *Mass Transfer in Heterogeneous Catalysis*, pp. 41, 42, M.I.T. Press, Cambridge, Mass., 1970.
7. O. Levenspiel: *Chemical Reaction Engineering*, chapt. 12, J. Wiley and Sons, New York, 1962.